HDL-TR-2082
April 1986

Experimental Determination of the Low-Energy Spectral Component of Cobalt-60 Sources

by Klaus G. Kerris
S. G. Gorbics

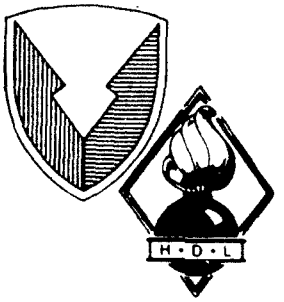

U.S. Army Laboratory Command
Harry Diamond Laboratories
Adelphi, MD 20783-1197

UNCLASSIFIED

SECURITY CLASSIFICATION OF THIS PAGE *(When Data Entered)*

REPORT DOCUMENTATION PAGE		READ INSTRUCTIONS BEFORE COMPLETING FORM
1. REPORT NUMBER HDL-TR-2082	2. GOVT ACCESSION NO.	3. RECIPIENT'S CATALOG NUMBER
4. TITLE *(and Subtitle)* Experimental Determination of the Low-Energy Spectral Component of Cobalt-60 Sources		5. TYPE OF REPORT & PERIOD COVERED Technical Report 6. PERFORMING ORG. REPORT NUMBER
7. AUTHOR*(s)* Klaus G. Kerris S. G. Gorbics (Naval Research Laboratory)		8. CONTRACT OR GRANT NUMBER*(s)*
9. PERFORMING ORGANIZATION NAME AND ADDRESS Harry Diamond Laboratories 2800 Powder Mill Road Adelphi, MD 20783-1197		10. PROGRAM ELEMENT, PROJECT, TASK AREA & WORK UNIT NUMBERS Program Ele: 6.21.20.A DA Project: 1L162120AH25
11. CONTROLLING OFFICE NAME AND ADDRESS U.S. Army Laboratory Command 2800 Powder Mill Road Adelphi, MD 20783-1145		12. REPORT DATE April 1986 13. NUMBER OF PAGES 42
14. MONITORING AGENCY NAME & ADDRESS*(if different from Controlling Office)*		15. SECURITY CLASS. *(of this report)* UNCLASSIFIED 15a. DECLASSIFICATION/DOWNGRADING SCHEDULE

16. DISTRIBUTION STATEMENT *(of this Report)*

Approved for public release; distribution unlimited.

17. DISTRIBUTION STATEMENT *(of the abstract entered in Block 20, if different from Report)*

18. SUPPLEMENTARY NOTES

HDL Project: XE7525
AMS Code: 612120.H250011

19. KEY WORDS *(Continue on reverse side if necessary and identify by block number)*

Dose enhancement
Cobalt-60 irradiator
Radiation hardness testing
Photon spectrum
Differential absorption spectrometer
Ionization chamber
Interface dose enhancement

20. ABSTRACT *(Continue on reverse side if necessary and identify by block number)*

A knowledge of the relative fraction of low-energy photons in the energy spectrum of cobalt-60 irradiators is essential to the proper interpretation of dosimetry and device test data in radiation response testing of electronic devices and circuits. It is shown that the relative magnitude of the low-energy spectral component of cobalt-60 gamma radiation can be determined experimentally by the use of a gold-and aluminum-walled air ionization chamber. The design and details of the construction of such a chamber are given. Experimental data from a large variety of cobalt-60 irradiator facilities are given and the

DD FORM 1 JAN 73 1473 EDITION OF 1 NOV 65 IS OBSOLETE

UNCLASSIFIED

SECURITY CLASSIFICATION OF THIS PAGE *(When Data Entered)*

20. ABSTRACT (cont'd)

facilities are ranked in order of their gamma spectrum hardness. Finally it is shown that the ionization chamber data can be used to calculate an upper limit on the expected interface dose-enhancement factor for a given material geometry.

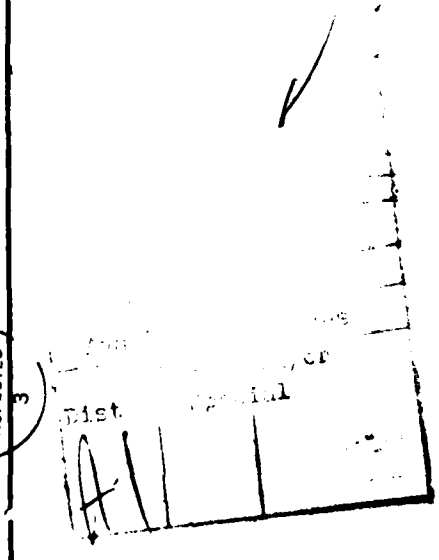

CONTENTS

APPENDICES

FIGURES

TABLES

1. INTRODUCTION

A number of recent papers[1-4] have pointed out that the gamma radiation from commonly used cobalt-60 sources is by no means limited to the monoenergetic photons at 1.17 and 1.33 MeV. The photon spectra of all practically realizable cobalt-60 irradiators include sizable low-energy Compton scattered components which, in some source configurations, can be very large indeed. The importance of low-energy photons to interface dose-enhancement effects, especially in semiconductor devices consisting of thin layers of materials of dissimilar atomic numbers, has also been described in a number of papers since 1970.[5-9] It is therefore clear that it is important to have some knowledge of the low-energy scattered gamma component of the particular cobalt-60 source which one is using for radiation effects testing of microelectronic devices and circuits. It is also unfortunately true, however, that this information is difficult to obtain. It is evident from recent experience with Monte-Carlo calculations of the gamma spectra of a few particular source configurations[3,4] that such calculations are extremely costly and time consuming. It is also not possible to draw general conclusions about the spectra of broad classes of cobalt-60 irradiators. Each specific configuration must be calculated individually.

In this paper we present an experimental method which gives a simple, easy, and direct method for determining the relative magnitude of the low-energy gamma component for any given cobalt-60 source geometry and experimental arrangement. It had been conjectured by a number of people for the past two years that measurement of the equilibrium dose using both a low-Z (Si, for example) and a high-Z (Au, for example) dosimeter of some kind would provide sufficient spectral information. In January of 1984, E. A. Burke* suggested that a thin air-ionization chamber with interchangeable aluminum and gold walls might be a practical implementation of such a pair of dosimeters. In this paper, we discuss the design of such an ionization chamber, present experimental data taken at a number of cobalt-60 facilities, and compare the experimental results with Monte-Carlo calculations of the spectra and with direct spectrum measurements using a novel dosimetric technique developed by one of the authors.

The detailed rationale of the design of the ionization chamber is discussed in section 2. Appendix A contains the complete fabrication drawings of the ionization chamber.

---

[1] L. F. Lowe, J. R. Capelli, and E. A. Burke, IEEE Trans. Nucl. Sci., NS-29 (1982), 1992.

[2] J. C. Garth, E. A. Burke, and S. Woolf, IEEE Trans. Nucl. Sci., NS-27 (1980), 1459.

[3] S. Woolf and A. R. Frederickson, IEEE Trans. Nucl. Sci., NS-30 (1983), 4371.

[4] S. Woolf and E. A. Burke, IEEE Trans. Nucl. Sci., NS-31 (1984), 1089.

[5] J. A. Wall and E. A. Burke, IEEE Trans. Nucl. Sci., NS-17, No. 6 (December 1970), 305.

[6] J. C. Garth, W. L. Chadsey, and R. L. Sheppard, Jr., IEEE Trans. Nucl. Sci., NS-22 (1975), 2562.

[7] W. L. Chadsey, IEEE Trans. Nucl. Sci., NS-25 (1978), 1591.

[8] D. B. Brown and C. M. Dozier, IEEE Trans. Nucl. Sci., NS-29 (1982), 1996.

[9] D. M. Long, D. G. Millward, and J. Wallace, IEEE Trans. Nucl. Sci., NS-29 (1982), 1980.

*E. A. Burke, Rome Air Development Center, L. G. Hanscom AFB, MA, 01731. Communicated at ASTM Subcommittee E-10.07 meeting, San Diego, CA, 25 January 1984.

Section 3 contains the theoretical derivation and experimental measurement of the energy response function of the ionization chamber.

Results of measurements of a variety of cobalt-60 irradiators with the ionization chamber are given in section 4. Section 5 presents the results of a direct measurement of some cobalt-60 irradiator spectra using a differential absorption technique. In section 6 the ionization chamber data of section 4 are compared with the results one would expect from the measured spectra, and with some calculated spectra from the recent literature.

Section 7 shows how the ionization chamber data can be related to the dose-enhancement factor near the boundary of two dissimilar materials. Appendix B contains a simple empirical model for calculating dose enhancement.

Finally in section 8 we conclude that the gold- and aluminum-walled ionization chamber is a simple and easy tool for qualitatively assessing the magnitude of the low-energy component of cobalt-60 irradiator spectra.

2. IONIZATION CHAMBER DESIGN

In order to make aluminum and gold equilibrium dose measurements at a large variety of cobalt-60 facilities, an ionization chamber should satisfy the following criteria:

(a) The walls (Al or Au) must be thick enough to establish charged-particle equilibrium at the location of the air-filled cavity.

(b) The cavity must be thin enough to satisfy the Bragg-Gray criterion; that is, the cavity dimensions must be small relative to the range of secondary electrons produced by photons in the wall material.

(c) The chamber should be useable over the range of exposure rates from 100 R/hr to 100 R/s. This means that the chamber response should be substantially linear with exposure rate up to 100 R/s. On the other hand, since the chamber is used only for relative measurements, its absolute calibration (in amperes per roentgen per second) need not be known precisely.

Wall and Burke[5] have shown that near an aluminum/gold interface, charged-particle equilibrium for cobalt-60 radiation is established 1000 μm into the aluminum and 50 μm into the gold. Therefore, to satisfy criterion a above, the aluminum dose measurement is made with 1500-μm (0.060 in.) thick aluminum walls. The gold dose measurement is made with 50-μm (0.002 in.) walls of gold on the cavity side, backed up with 1500 μm of aluminum on the outside.

[5] J. A. Wall and E. A. Burke, IEEE Trans. Nucl. Sci., NS-17, No. 6 (December 1970), 305.

In order to satisfy criteria b (thin air cavity) and c (good sensitivity at 100 R/hr) we decided to use a parallel-plate geometry for the chamber. The collecting efficiency for a parallel-plate ionization chamber is given by[10,11]

$$f = \left(1 + m^2 q d^4 / 6V^2\right)^{-1} \qquad (1)$$

where

f = charge collected/charge generated,
m = Boag's constant = 36.7 ± 2.2 for air at standard temperature and pressure,
q = ionization rate (esu/cm^3-s),
d = electrode spacing (cm),
V = collecting voltage (V).

From the definition of the roentgen (1 R ≡ 1 esu/cm^3), we see that 1 esu/cm^3-s = 1 R/s. Therefore, we can substitute the exposure rate, $\dot{X}$ (in roentgens per second), for q in equation (1). Criterion b requires that d be ≤3 mm, since the range of 10-keV electrons in air is 2.4 mm. If we require that $f \geq 0.95$ for $\dot{X} \leq 100$ R/s (criterion c), then equation (1) will be satisfied for d = 3 mm and V = 60 V.

The collected ionization current of a parallel-plate ionization chamber is given by[12]

$$I = 3.33 \times 10^{-10} f \dot{X} A d \quad , \qquad (2)$$

where

f = collection efficiency,
$\dot{X}$ = exposure rate (R/s),
A = area of cavity (cm^2), and
d = thickness of cavity (cm).

Since tens of picoamperes are easy to measure reliably, a chamber sensitivity of 1 nA/R-s^{-1} will satisfy the sensitivity criterion c at 100 R/hr. A cavity diameter, D, of 4 cm, d = 3 mm, and f ≈ 1 gives a chamber sensitivity of 1.26 nA/R-s^{-1}.

In summary then, an ionization chamber satisfying all these criteria would have the following specifications:

---

[10] T. E. Burlin, The Theory of Dosimeter Response with Particular Reference to Ionization Chambers, chapter II in Manual on Radiation Dosimetry, ed. by N. W. Holm and R. J. Berry, Marcel Dekker Inc., New York (1970), p 27.

[11] J. W. Boag, Ionization Chambers, chapter 9 in Radiation Dosimetry, ed. by F. H. Attix and W. C. Roesch, 2nd edition, vol. II, Academic Press, New York (1966), p 16.

[12] R. D. Evans, The Atomic Nucleus, McGraw-Hill, New York (1955), p 725.

cavity diameter, D = 4.0 cm
electrode spacing, d = 0.3 cm
bias voltage, V = 60 V
Al wall thickness = 0.060 in. of Al
Au wall thickness = 0.002 in. of Au, backed by 0.060 in. of Al

This chamber will have the following collection efficiencies and approximate calibration:

At X = 100 R/s: f = 0.95 and $I/\dot{X}$ = 1.20 nA/R-s^{-1}
At X $\lesssim$ 9.7 R/s: f = 1.00 and $I/\dot{X}$ = 1.26 nA/R-s^{-1}

An exploded view of the ionization chamber is shown in figure 1 (complete drawings are given in app A). The chamber body is made from polystyrene to minimize leakage currents. No guard ring is used because the 4.0 : 0.3 cm aspect ratio is very high and because it is not necessary to know the absolute calibration of the chamber. Connection from the Trompeter TWC 78-2 twinaxial cable to the chamber electrodes is by mechanical pressure from the electrode cover plates.

The 60-V bias was provided by a Hewlett-Packard Model 6212B 0- to 100-V dc power supply. The ionization current was measured by a Keithley Model 614 digital electrometer. The resolution of the electrometer is +0.01 pA on its most sensitive range, making current measurements of tens of picoamperes quite feasible and accurate.

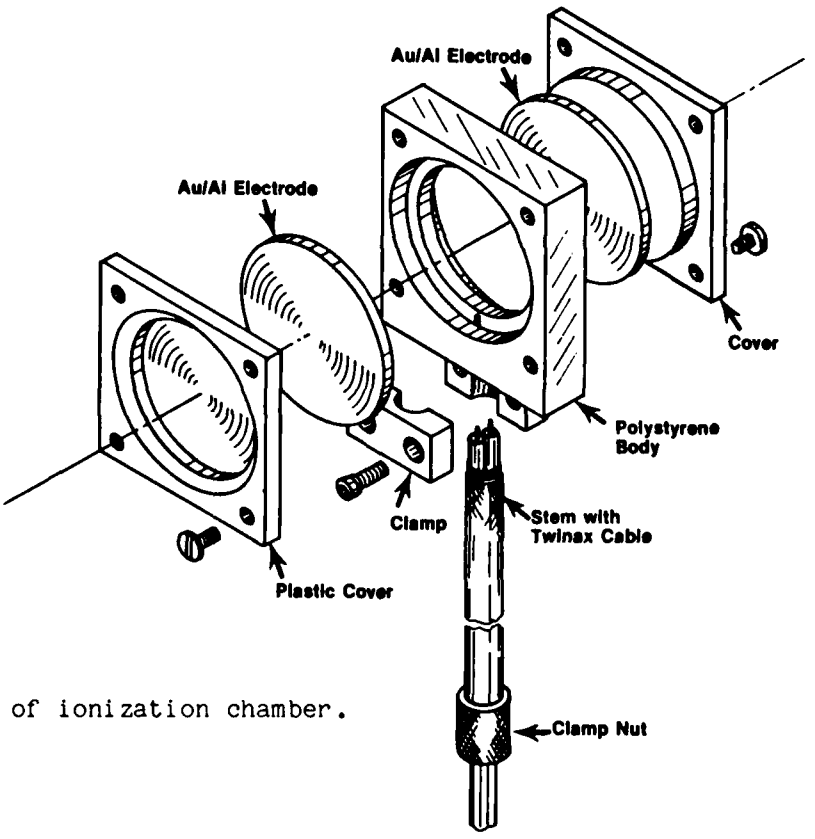

Figure 1. Exploded view of ionization chamber.

3. ENERGY RESPONSE FUNCTION

Spectral quality measurements of a cobalt-60 source using the gold/aluminum ionization chamber are made as follows. Using the 0.060-in. aluminum electrodes, the ionization current, I_{Al}, is measured at the experimental position of interest. Next, the 0.002-in. gold + 0.060-in. aluminum electrodes are inserted (gold on the inside) and the ionization current, I_{Au}, is measured at the same position. The ratio I_{Au}/I_{Al} is indicative of the spectral purity of the gamma radiation.

In order to compare the measured I_{Au}/I_{Al} response with the theoretical prediction for a given photon spectrum, it is necessary to know the monoenergetic photon energy response function $S(E) \equiv I_{Au}(E)/I_{Al}(E)$ for the ionization chamber.

3.1 Theoretical Derivation

The Bragg-Gray equation for an ionization chamber is[13]

$$D_m = Q_g(\bar{W}/e)\bar{s}_{mg} \quad , \tag{3}$$

where

D_m = dose in an irradiated medium, m, near a small cavity filled with a gas, g,

Q_g = ionization charge/unit mass in the gas
= (collected charge/f)/(cavity volume × density of gas, ρ_g),

$\bar{W}$ = energy expended per ion-pair formed
= 33.75 ± 0.15 eV/ion-pair,

e = charge of electron, and

$\bar{s}_{mg}$ = average mass stopping power ratio*
$= \bar{S}_m/\bar{S}_g$
$= R_g(E_\gamma)/R_m(E_\gamma)$.

---

[13] Radiation Dosimetry: X-Rays and Gamma Rays with Maximum Photon Energies Between 0.6 and 50 MeV, International Commission on Radiation Units and Measurements, ICRU Report 14, Washington (1969), p 4.

*In the continuous-slowing-down-approximation (csda), the mass stopping power S(E) is given by

$$f(E) = 1/S(E) \quad ,$$

where

f(E) = electron spectrum ($g\text{-}cm^{-2}\text{-}MeV^{-1}$) , S(E) = mass stopping power ($MeV\text{-}cm^2\text{-}g^{-1}$) .

The average mass stopping power is then given by

$$\bar{S} = \int_0^{E_{max}} S(E)f(E)\,dE \Big/ \int_0^{E_{max}} f(E)\,dE$$

$$= E_{max}/R(E_{max}) \quad ,$$

where $R(E_{max})$ is the range of electrons of energy E_{max}. Therefore, for secondary electrons, $\bar{S} \propto 1/R(E_\gamma)$, except near a K-absorption edge where one should use $R(E_\gamma - K_{abs})$.

If the cavity is filled with air, we can rewrite equation (3):

$$\dot{D}_m = J_g(\bar{W}/e)(R_{air}/R_m) \quad , \tag{4}$$

where

J_g = ionization current/unit mass
= (observed current/f)/(cavity volume × ρ_{air})
= $I_m/fAd\rho_{air}$.

Equation (4) becomes

$$\dot{D}_m = KI_m(R_{air}/R_m) \quad , \tag{5}$$

where

$$K \equiv \bar{W}/efAd\rho_{air} \quad , \tag{6}$$

which is a constant depending only on ionization chamber parameters. Solving equation (5) for I_m gives

$$I_m = K^{-1}\dot{D}_m(R_m/R_{air}) \quad , \tag{7}$$

which is the observed current in an air-filled ionization chamber of wall material m, when the absorbed dose rate in the wall material near the cavity is $\dot{D}_m$.

Now, for the case of charged particle equilibrium

$$\dot{D}_m = \dot{\Phi}_\gamma(\mu_{en}/\rho)_m \quad , \tag{8}$$

where

$\dot{\Phi}_\gamma$ = photon energy fluence rate (MeV-cm^{-2}s^{-1}) and
μ_{en}/ρ = mass energy absorption coefficient (cm^2/g).

For thick chamber walls

$$\dot{\Phi}_\gamma = \dot{\Phi}_o \exp[-(\mu_{en}/\rho)_w\rho_w t_w] \quad , \tag{9}$$

where

$\dot{\Phi}_o$ = incident photon energy fluence rate,
$(\mu_{en}/\rho)_w$ = mass energy absorption coefficient of walls,
ρ_w = density of walls (g/cm^3), and
t_w = thickness of walls (cm).

For the two configurations of our ionization chamber, combining equations (7), (8), and (9), we have

$$I_{Al} = K^{-1}\dot{\Phi}_o \exp[-(\mu_{en}/\rho)_{Al}\rho_{Al}t_{Al}](\mu_{en}/\rho)_{Al}(R_{Al}/R_{air}) \quad (10a)$$

and

$$I_{Au} = K^{-1}\dot{\Phi}_o \exp[-(\mu_{en}/\rho)_{Al}\rho_{Al}t_{Al} - (\mu_{en}/\rho)_{Au}\rho_{Au}t_{Au}] \times (\mu_{en}/\rho)_{Au}(R_{Au}/R_{air}) \quad . \quad (10b)$$

Division of equation (10b) by equation (10a) gives the monoenergetic photon response function $S(E) = I_{Au}(E)/I_{Al}(E)$:

$$S(E) = \frac{(\mu_{en}/\rho)_{Au}}{(\mu_{en}/\rho)_{Al}} \frac{R_{Au}}{R_{Al}} \exp[-(\mu_{en}/\rho)_{Au}\rho_{Au}t_{Au}] \quad . \quad (11)$$

The electrodes of the ionization chamber were made from aluminum alloy 7075. We assumed the following composition for this alloy:

Al:	0.901
Zn:	0.056
Mg:	0.025
Cu:	0.016
Cr:	0.002

Using values of μ_{en}/ρ tabulated by Evans[14] and Hubbell[15] and values of R tabulated by Berger and Seltzer,[16] as well as the experimentally determined value of

$$\rho_{Au}t_{Au} = 0.0974 \text{ g/cm}^2$$

for the gold foil covering on the Al + Au electrodes, we calculate the energy response function shown by the solid line in figure 2.

3.2 Experimental Determination

The monoenergetic response function of the actual chamber was also measured directly at the five points indicated by circles in figure 2. These measurements were made with a heavily filtered x-ray source of x-ray energies of 38, 70, 113, 169, and 206 keV. The dashed line in figure 2 is the best smooth-curve fit through these five experimental points.

---

[14] R. D. Evans, X-Ray and γ-Ray Interactions, chapter 3 in Radiation Dosimetry, ed. by F. H. Attix and W. C. Roesch, ed., 2nd edition, vol I, Academic Press, New York (1968), p 125 ff.

[15] J. H. Hubbell, Trends in Radiation Dosimetry, 33, No. 11 (November 1982).

[16] M. J. Berger and S. M. Seltzer, Tables of Energy Losses and Ranges of Electrons and Positrons, National Aeronautics and Space Administration, NASA SP-3012, Washington (1964).

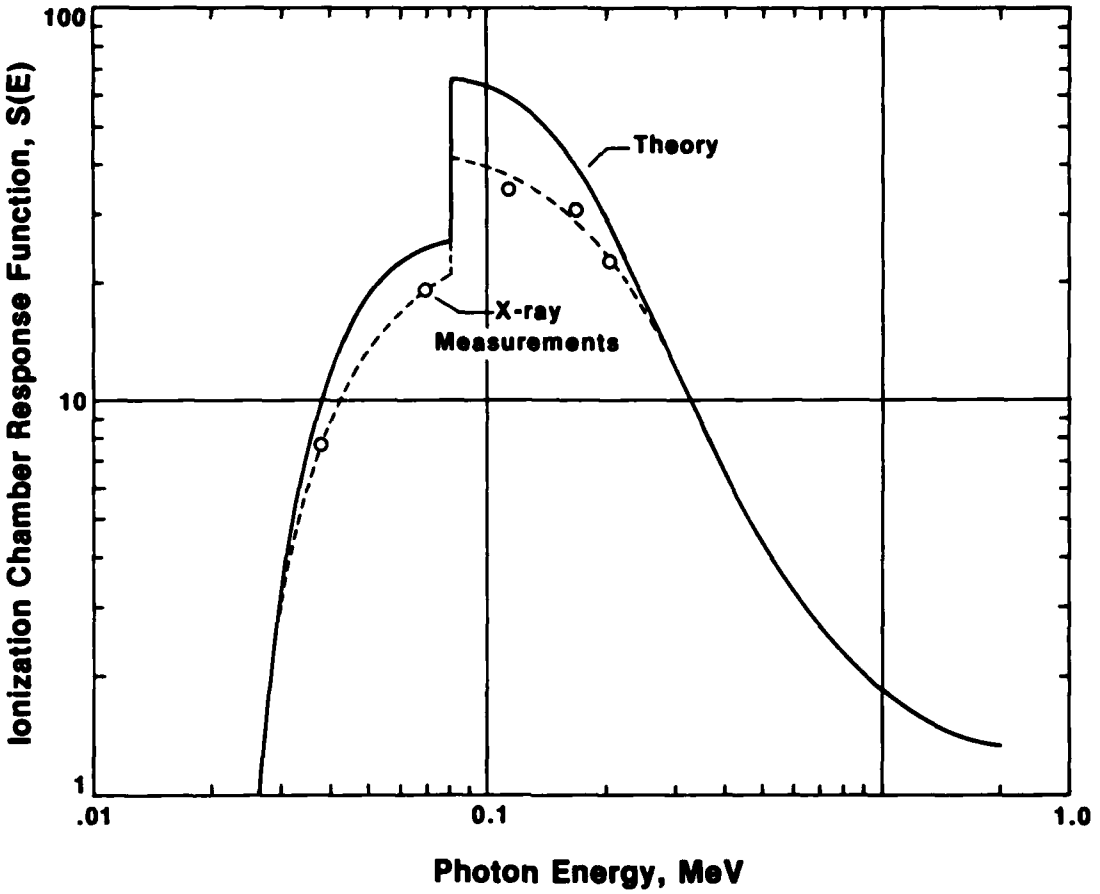

Figure 2. Ionization chamber energy response function.

We attribute the discrepancy between the calculated and experimental curves to these factors:

(a) The actual metallurgical composition of our aluminum plates is not known. In particular, a higher fraction of zinc and copper would lower the calculated value of S(E).

(b) The air volume thickness of 3 mm does not approximate the Bragg-Gray condition very well at low photon energies. We verified this by repeating the filtered x-ray measurements for air volume thicknesses of 4 and 5 mm. These measurements showed that better agreement between the two curves would result from the use of an electrode spacing considerably less than 3 mm. However, such an ionization chamber would be impractical to use. Moreover, for the purposes of cobalt-60 source testing, it is not very important to achieve exact agreement of this chamber parameter with theory, as long as we know the actual measured value.

(c) The approximation that $\bar{S}(E_e) = E_{max}/R(E_{max})$ is not very good near the K-absorption edge of gold at 80.8 keV.

The important point to note here is that the ionization chamber response ratio for pure cobalt-60 gamma radiation (E_γ = 1.25 MeV) would be 1.6. Also note that very little scattered radiation of lower energy would be expected to cause a significant increase in the chamber response ratio, since the response function is close to 40 at $E_\gamma \approx 100$ keV. We would, therefore, expect this I_{Au}/I_{Al} measurement to provide a very sensitive indication of the purity of a cobalt source spectrum.

4. EXPERIMENTAL RESULTS

Various cobalt-60 sources were investigated with the ionization chamber in a number of typical experimental configurations. These sources are described briefly below.

4.1 Water Well Sources

In a typical water well source, the cobalt-60 elements are at the bottom of a water-filled well which provides shielding for personnel protection. Source elements are usually slender cylindrical rods which are arranged around the periphery of a cylindrical exposure volume. Objects to be irradiated are enclosed in a water-tight thin-walled stainless steel container which is lowered into the exposure volume, displacing most of the water. This arrangement is illustrated diagrammatically in figure 3(a). Some facilities also have provisions for placing the exposure canister outside the cobalt-60 array, using some of the intervening water to reduce the exposure rate in the canister. This arrangement is shown in figure 3(b). Water well irradiators were tested in various configurations at the U.S. Army Harry Diamond Laboratories (HDL), the Naval Research Laboratory (NRL), and the National Bureau of Standards (NBS).

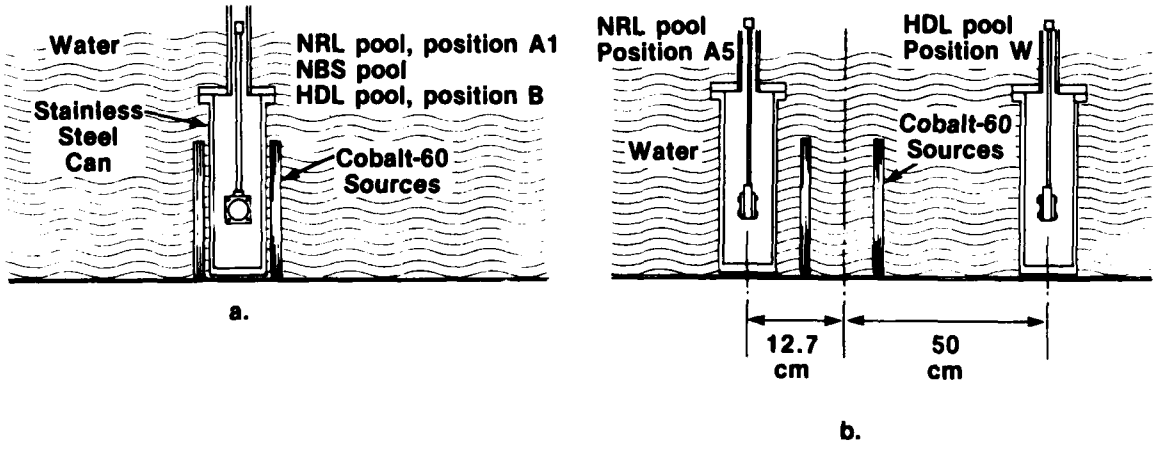

Figure 3. Water well irradiator: (a) detector surrounded by Co^{60} sources and (b) detector outside Co^{60} sources.

4.2 Concrete Rooms

Some facilities consist of a large concrete room in which the test object is arranged. A cobalt-60 source is then exposed, either by lifting it out of a lead or water shield or by opening a lead shutter. Two such sources which were investigated are at HDL and at the NASA Goddard Space Flight Center (NASA).

At the HDL facility, the source array is lifted from a water well approximately into the center of a 40-ft long by 12-ft high concrete room. Two experimental arrangements were investigated:

(a) ionization chamber in center of room, about 30 cm from the source array;

(b) ionization chamber 30 cm from the back wall and 75 cm from the ceiling of this room.

These two arrangements are shown diagrammatically in figure 4(a).

The NASA facility consists of a 20 by 20 ft concrete room. The cobalt source is a plane array, 9 by 18 in., approximately in the center of one wall. The source array is exposed by lifting a massive lead shutter. Ionization chamber locations were approximately 35 cm from the source and 35 cm from the rear wall of the chamber. This arrangement is shown diagrammatically in figure 4(b).

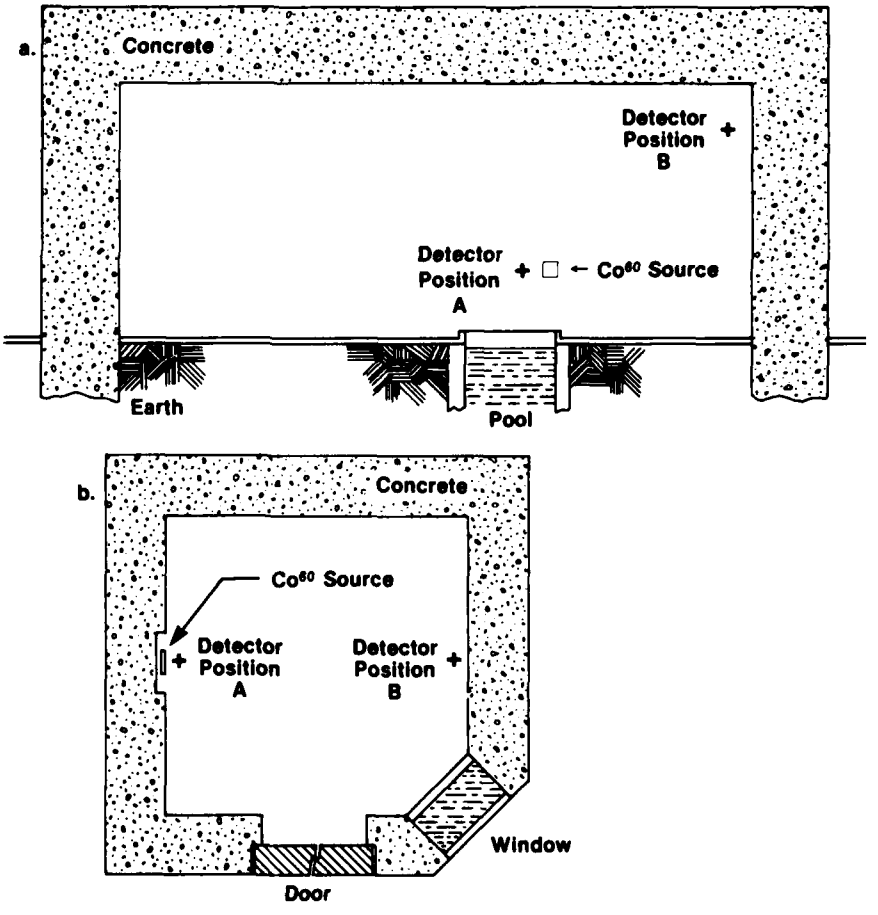

Figure 4. Concrete room irradiation facilities: (a) HDL (elevation) and (b) NASA (plan view).

4.3 Lead-Shielded Sources

Two facilities have cobalt-60 sources inside lead shields.

The NBS vertical teletherapy source has an adjustable collimator and a lead shutter, allowing the gamma rays to shine into a low-scatter hot cell.

The NASA source is a commercial Gammacell™-220 irradiator manufactured by AEC-Canada, Ltd. In this irradiator the source rods surround a cylindrical cavity at the center of a large lead shield. The test object (ionization chamber) is lowered into the center of this shield.

These two sources are illustrated diagrammatically in figure 5.

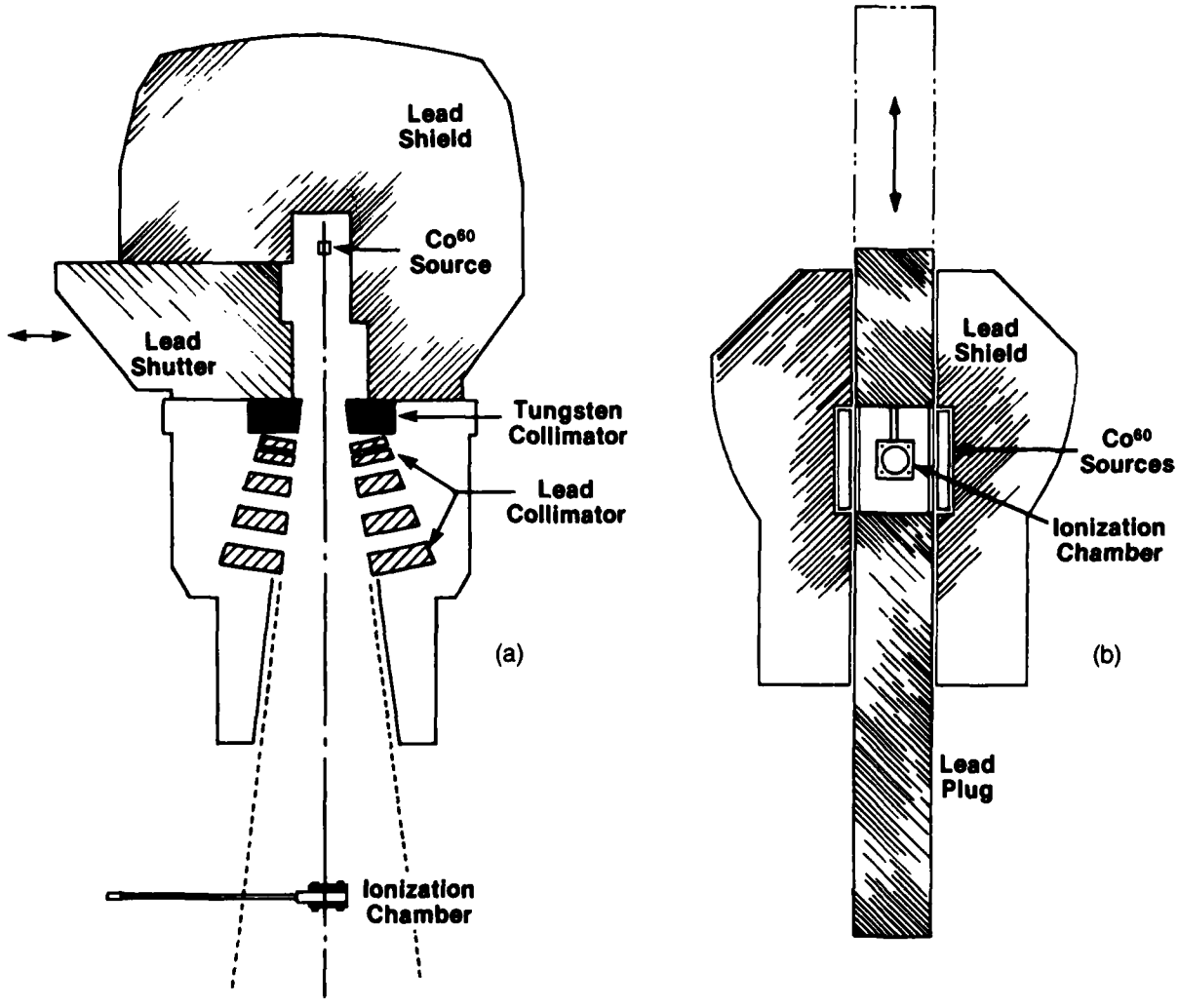

Figure 5. Lead-shielded sources: (a) NBS teletherapy source and (b) NASA Gammacell™-220.

Brown and Dozier[8] have recommended that whenever a significant low-energy gamma component is expected, microelectronic circuits and components be tested in a shield box made of 0.063-in.-thick lead (on the Co^{60} side) and 0.030 in. of aluminum (on the test-object side). This filter box will harden the spectrum by selectively attenuating the low-energy scattered component of the radiation while not attenuating the primary gamma rays significantly. Accordingly, all ionization chamber measurements were made with and without a lead-aluminum filter.

The experimentally determined values of I_{Au}/I_{Al}, with and without lead-aluminum filters, are presented in table 1 for the cobalt-60 source configurations of figures 3 to 5. Note that the NBS teletherapy source emits the cleanest spectrum (I_{Au}/I_{Al} = 2.18) as expected, and that the expected high-scatter geometries (concrete room positions B and water well position W) gave very high values of I_{Au}/I_{Al} of 6.2 to 7.6. Also note that the ionization chamber response for most filtered source configurations is as good as or better than the best unfiltered source geometry.

TABLE 1. EXPERIMENTALLY DETERMINED VALUES OF IONIZATION CHAMBER RESPONSE RATIO, I_{Au}/I_{Al}

Line No.	Cobalt-60 source configuration				Unfiltered I_{Au}/I_{Al}	Filter		Filtered I_{Au}/I_{Al}
	Place	Type	Position	Figure		Pb (in.)	+ Al (in.)	
1	NRL	Water well	A1	3a	2.71	0.073	0.017	2.02
2	NBS	Water well	--	3a	2.98	0.063	0.030	2.04
3	HDL	Water well	B	3a	3.23	0.063	0.030	2.11
4	NRL	Water well	A5	3b	3.86	0.073	0.017	2.28
5	HDL	Water well	W	3b	7.40	0.063	0.125	3.53
6	HDL	Concrete room	A	4a	2.70	0.063	0.000	2.12
7	HDL	Concrete room	B	4a	7.56	0.125	0.030	2.52
8	NASA	Concrete room	A	4b	2.93	0.063	0.030	2.21
9	NASA	Concrete room	B	4b	6.17	0.063	0.030	3.27
10	NBS	Teletherapy source	--	5a	2.18	0.063	0.030	2.07
11	NASA	Gammacell™-220	--	5b	3.53	0.063	0.030	2.17

5. DIRECT MEASUREMENT OF COBALT-60 SOURCE SPECTRA

The spectra of the scattered radiation of some of the sources were measured by a differential absorption spectrometer. The use of differential absorption by materials of differing Z and graded thicknesses to deduce photon spectra in situations where pulse-height analysis is difficult or impossible is not a new concept. Various investigators have used absorption "stacks" to provide data which are then unfolded to yield the presumed incident spectrum. This type of spectrometry is especially useful for the measurement of pulsed bremsstrahlung fields where high-intensity, short-duration radiation pulses are produced or, as in this case, where the radiation intensity cannot be

[8] D. B. Brown and C. M. Dozier, IEEE Trans. Nucl. Sci., NS-29 (1982), 1996.

reduced to low enough levels for the use of methods which involve pulse counting. The system used in these measurements has been devised to overcome some of the difficulties inherent in previous spectrometers of this type.

5.1 Description of Differential Absorption Spectrometer

The spectrometer consists of a series of spherical shells each of which contains a central cavity 3/8 in. in diameter. The shells range in thickness from 1/16 to 9/16 in. and are made from aluminum, titanium, copper, and depleted uranium. In use, each cavity contains a CaF_2:Mn thermoluminescent dosimeter (TLD) (Harshaw Chemical Co., TLD-400) wrapped in a single layer of 1-mil aluminum foil. The materials and thicknesses are chosen to give a series of absorption curves whose low-energy cutoffs are spaced reasonably uniformly over the logarithmic range of energies available.

The detector response function of each of the spheres as a function of energy, calculated from their energy-absorption coefficients, is shown in figure 6. The measured energy dependence of the TLD detectors and the dose enhancement due to the lack of electronic equilibrium have been included in the figure. A series of measurements with standard heavily filtered x-ray spectra and cesium-137 and cobalt-60 gamma-ray sources was used to check the validity of the absorption calculations and, for the depleted uranium spheres, to adjust them for the over-response caused by the high Z of the shield. These measurements provided experimental checks at 38, 70, 117, 169, 206, 663, and 1250 keV. In all cases except for the uranium shells, the agreement between the measured and calculated response curves is quite good, and these curves are used as the final response functions. The paucity of energy calibration points at the higher energy regions required empirical adjustment of the uranium response functions. Their magnitudes were adjusted to give a minimum error in the unfolding code for the spectrum with the smallest low-energy component.

5.2 Principle of Operation

Some specific attributes of this spectrometer make its use feasible in this application. The TLD's used can be calibrated to a precision of about 1-1/2 percent. Such high precision facilitates the spectrum-unfolding process and removes the need for larger numbers of dosimeters, as have been used in previous absorption spectrometers. The high sensitivity and wide dose range of these detectors allow measurements of widely varying x- and gamma-radiation fields. The fact that each individual TLD is positioned at the center of a spherical shell reduces the directionality of the spectrometer. The absorbers are not connected in a "stack" but remain individual and can be changed at will. Though the set of absorption spheres is normally used in a group for an irradiation, the versatility of this geometry allows them to be singly irradiated in the limited space within the cobalt-60 pool irradiation cans, with each sphere placed in the proper position in turn.

The general method of differential absorption spectrometry does have some unavoidable problems, however. There is an upper energy limit to its

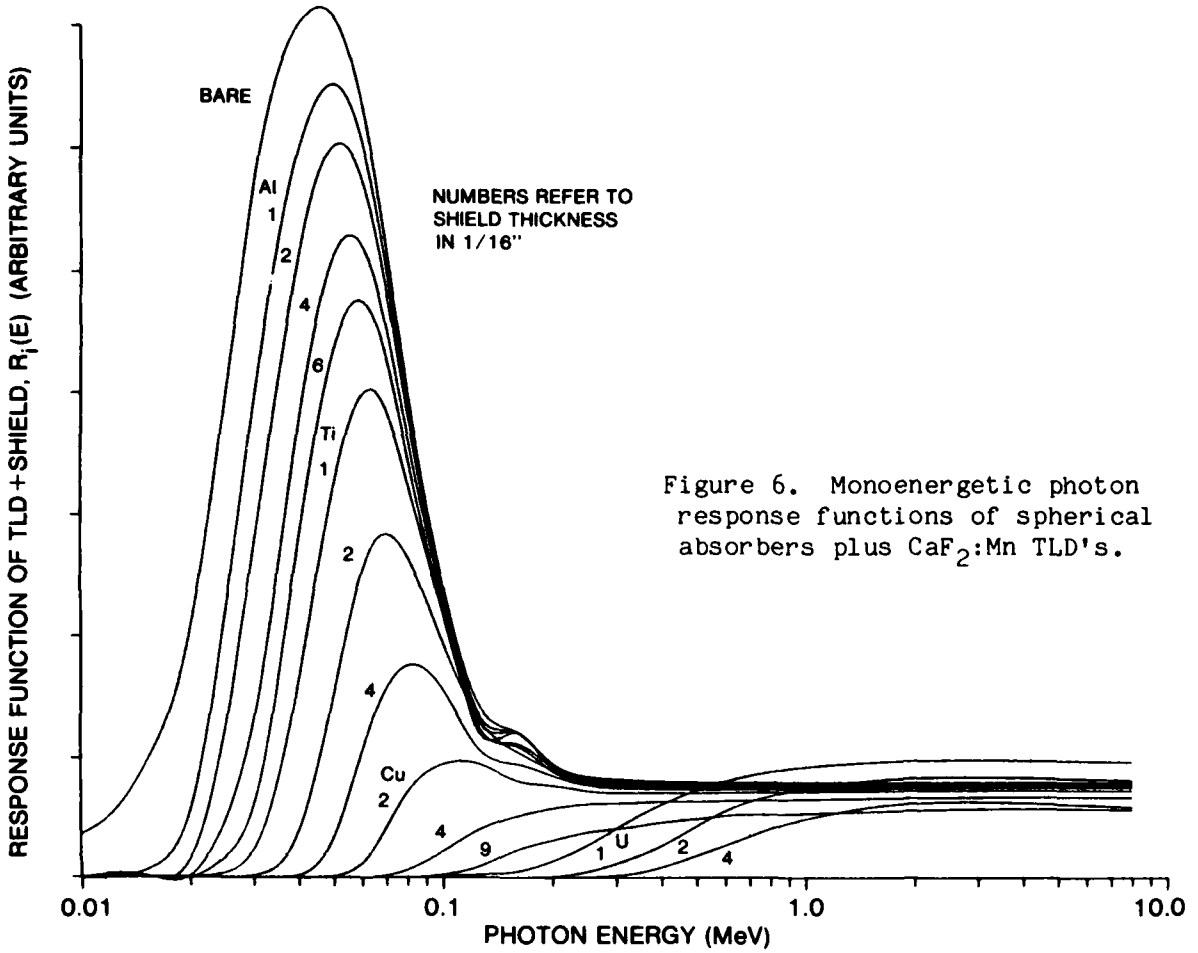

Figure 6. Monoenergetic photon response functions of spherical absorbers plus CaF_2:Mn TLD's.

usefulness, since even the highest Z materials do not have sufficient variations in their absorption coefficients to be useful above a few hundred kiloelectronvolts. Specifically, such a spectrometer is most sensitive and responsive for measurements in the low-energy region (10 to 500 keV) but in the present application, there are drawbacks for its most efficient use even at these lower energies. In a spectrum where most of the energy lies above an energy region of interest, unfolding the lower energy portion of the spectrum must, by the nature of the response function shapes, depend on differences between large numbers. Each detector responds to all the radiation above some cutoff, as determined by the shape of the response function.

Though the details of the spectrum in the low-energy region will be in doubt through such a fit, the amount of energy that is parceled to each energy region will be useful in calculating field parameters. Since the measurement consists of determining the energy that is transmitted through various filters (essentially a measurement of dose as a function of depth--a depth-dose curve of sorts), the code will give consistent results when fitting the energy distributions to the accuracy that is possible. Using such energy distributions to determine derived quantities (such as rads in silicon) does

give relatively reliable results. However, since such quantities depend more strongly on the specific shape of the spectrum in the low-energy region, they will not be as consistent as the total energy results. Calculated values for exposure (roentgens) are quite reliable, since the response of air does not vary as sharply in the low-energy region as does that of silicon or higher Z materials.

5.3 Unfolding Code

An integral part of any differential absorption spectrometer is the unfolding code that is employed to recover the unknown spectrum. This system makes use of an iterative perturbation code developed for use in unfolding neutron spectra from Bonner sphere data. The code, titled YOGI, gives exceptionally stable solutions and allows the imposition of constraints, such as varying degrees of smoothing, nonnegative solutions, and the initial input of best-guess spectra. Such constraints facilitate the determination of "appropriate" solutions (solutions with physically reasonable shapes). The method and basic concept are the same in measurements involving Bonner sphere neutron or differential absorption x-ray data even though the response functions have a different form.

The equation

$$Q_i = \int S(E)R_i(E)\, dE \tag{12}$$

describes the response of the i^{th} detector, Q_i, to the spectrum to be determined, S(E), through the response function, $R_i(E)$. Reduced to j finite energy bins, the problem becomes the solution of i equations in j unknowns for the spectrum values, S_j, that best fit the input data consisting of the detector responses, Q_i, and the response function, R_{ij}:

$$Q_i = \sum_j S_j R_{ij}\, \Delta E_j \quad . \tag{13}$$

The code, YOGI, solves the equations by being given a starting spectrum (the more reasonable, the better) and calculating a set of Q_j's which are compared with the measured values to determine an error parameter such as the sum of the squares of the differences. The code then proceeds to perturb one point in the trial spectrum by some fixed amount, recalculate the error, and keep the perturbed value if the error has been improved. If not, that perturbation is rejected. The perturbation procedure is then repeated in random spectral energy bins until some given condition of fit has been met. The resulting spectrum is then considered a solution to the equations. Such a solution may not be a unique or even an "appropriate" one. To some extent, the solution depends on the initial input spectrum but even more so on constraints that are imposed by the code. One such constraint is the imposition of a certain amount of smoothing on the solution. Without smoothing, the solution can vary widely from point to point, a condition which is physically unreasonable and thus "inappropriate."

5.4 Experimental Results

The differential absorption spectrometer was used to measure the gamma spectra of seven of the cobalt-60 source configurations of table 1. These results are discussed in section 6, and illustrations are given.

6. COMPARISON OF IONIZATION CHAMBER DATA WITH CALCULATED AND MEASURED SPECTRA

Let $\phi(E)$ be the differential photon energy spectrum (in units of MeV/MeV) of any given cobalt-60 source, and let $S(E)$ be the energy response function of the ionization chamber as defined in equation (11). Then the expected ionization chamber response ratio, I_{Au}/I_{Al}, will be given by

$$\frac{I_{Au}}{I_{Al}} = \frac{\int S(E)\phi(E)\, dE}{\int \phi(E)\, dE} \quad . \tag{14}$$

This expected response was calculated for all source configurations for which either a calculated or measured spectrum was available, and was compared with the measured ionization chamber response.

6.1 Monte-Carlo Calculations

The gamma spectra of the source configurations corresponding to lines 2, 5, 6, 7, and 11 of table 1 have been calculated by S. Woolf using a Monte-Carlo transport code.[3,4] These spectra are shown in figure 7 (p 22). The ionization chamber energy response function of figure 2 was integrated over each of these eight spectra to find the expected ionization chamber response ratio, I_{Au}/I_{Al}. These calculated responses are compared with the measured values in table 2. The agreement is good, with a mean variation from the measured responses of -21 percent.

TABLE 2. COMPARISON OF MEASURED VALUES OF I_{Au}/I_{Al} WITH THOSE CALCULATED FROM MONTE-CARLO SPECTRA (ref 3,4)

Line No.	Cobalt-60 source configuration				Filter		Measured I_{Au}/I_{Al}	Calculated I_{Au}/I_{Al}	Figure[b]
	Place	Type	Position	Figure[a]	Pb (in.)	Al (in.)			
2	NBS	Water well	--	3a	(Unfiltered)		2.98	2.71	7g
5	HDL	Water well	W	3b	(Unfiltered)		7.40	4.48	7a
					0.063	0.125	3.53	2.80	7b
6	HDL	Concrete room	A	4a	(Unfiltered)		2.70	2.15	7c
					0.063	0.000	2.12	1.77	7d
7	HDL	Concrete room	B	4a	(Unfiltered)		7.56	4.92	7e
					0.125	0.030	2.52	1.94	7f
11	NASA	Gammacell™-220	--	5b	(Unfiltered)		3.53	3.40	7h

[a]Figure showing source configuration.
[b]Figure showing calculated spectrum.

[3]S. Woolf and A. R. Frederickson, IEEE Trans. Nucl. Sci., NS-30 (1983), 4371.
[4]S. Woolf and E. A. Burke, IEEE Trans. Nucl. Sci., NS-31 (1984), 1089.

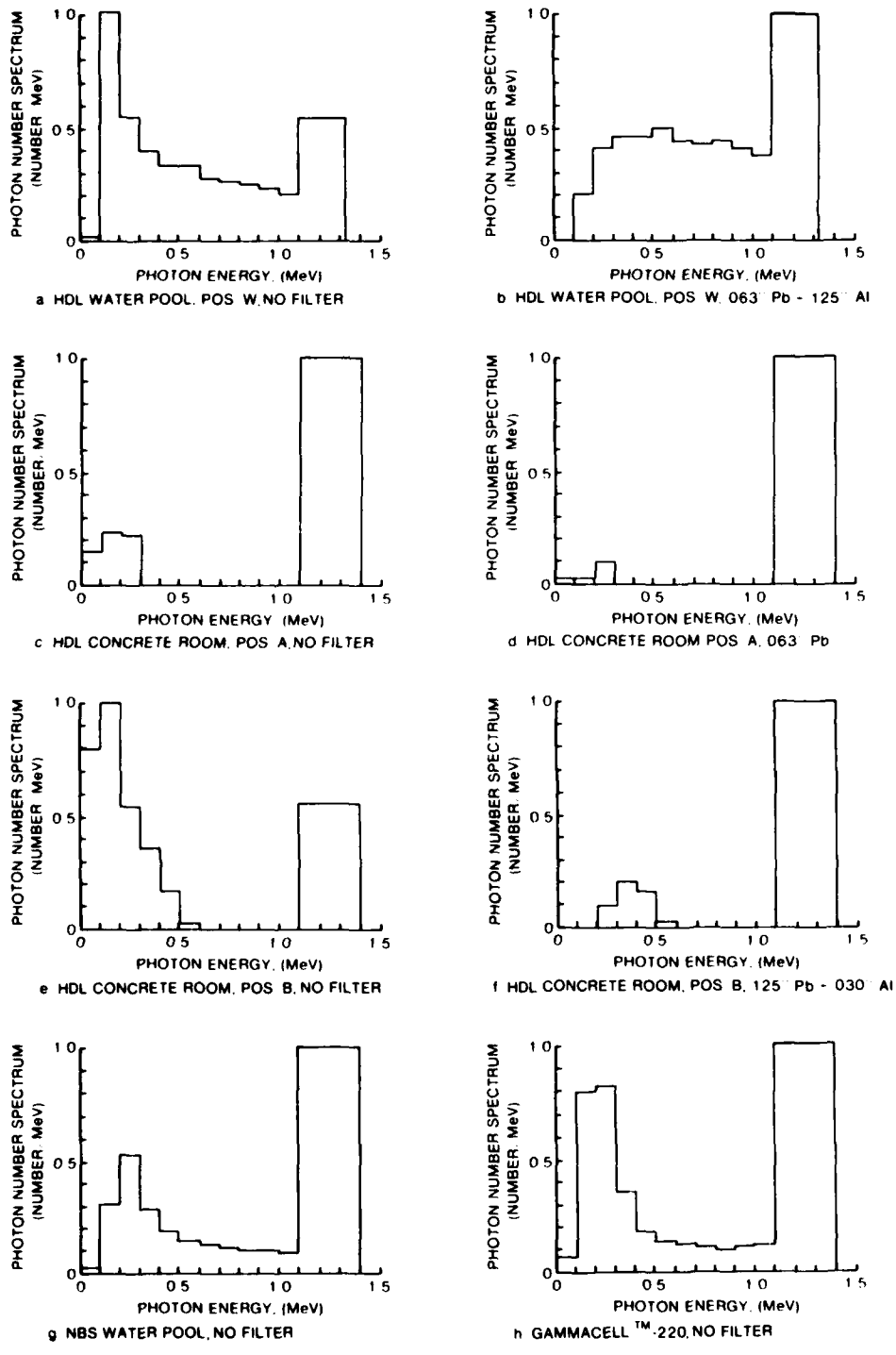

Figure 7. Calculated cobalt-60 source spectra (from S. Woolf et al, ref 3, 4).

6.2 TLD Differential Absorption Measurements

The ionization chamber response function (fig. 2) was also integrated over the gamma spectra which were measured for source configurations corresponding to lines 1, 5, 6, and 7 of table 1. These measured spectra are shown in figure 8 (p 24). The calculated responses are compared with the measured values in table 3. Again there is good agreement, with a mean variation from the measured values of -18 percent.

TABLE 3. COMPARISON OF MEASURED VALUES OF I_{Au}/I_{Al} WITH THOSE CALCULATED FROM MEASURED COBALT-60 SPECTRA

Line No.	Cobalt-60 source configuration				Filter		Measured I_{Au}/I_{Al}	Calculated I_{Au}/I_{Al}	Figure[b]
	Place	Type	Position	Figure[a]	Pb (in.)	+ Al (in.)			
1	NRL	Water well	A1	3a	(Unfiltered)		2.71	1.89	8a
					0.073	0.017	2.02	1.84	8b
5	HDL	Water well	W	3b	(Unfiltered)		7.40	7.09	8g
6	HDL	Concrete room	A	4a	(Unfiltered)		2.70	1.89	8c
					0.063	0.000	2.12	1.84	8d
7	HDL	Concrete room	B	4a	(Unfiltered)		7.56	5.56	8e
					0.125	0.030	2.52	2.17	8f

[a]Figure showing source configuration.
[b]Figure showing measured spectrum.

6.3 Relative Rankings

If we use the measured value of I_{Au}/I_{Al} as a relative figure of merit for the hardness of a cobalt-60 spectrum, with lower I_{Au}/I_{Al} values denoting spectra with smaller low-energy scattered components, then we can rank the sources listed in table 1 by this parameter. Table 4 is a rearrangement of the unfiltered source spectra in order of increasing I_{Au}/I_{Al}. The column headed "Quality factor" contains an entirely arbitrary parameter defined as follows:

Quality factor	I_{Au}/I_{Al}
I	≤2.50
II	2.51 to 3.00
III	3.01 to 4.00
IV	≥4.01

The NBS teletherapy source (line 10) is clearly in a class by itself. At the other end of the spectrum, the anticipated high-scatter configurations (lines 5, 7, and 9) are equally clearly very bad. All others are grouped somewhere between these extremes. If we now do a similar ranking on the filtered spectra, we see the spectacular improvement shown in table 5. All sources which had previously been in groups II and III are now in group I, with all but two having a harder spectrum than the best unfiltered source: the NBS teletherapy source. No useful conclusion can be drawn from group IV; line 7 moved from

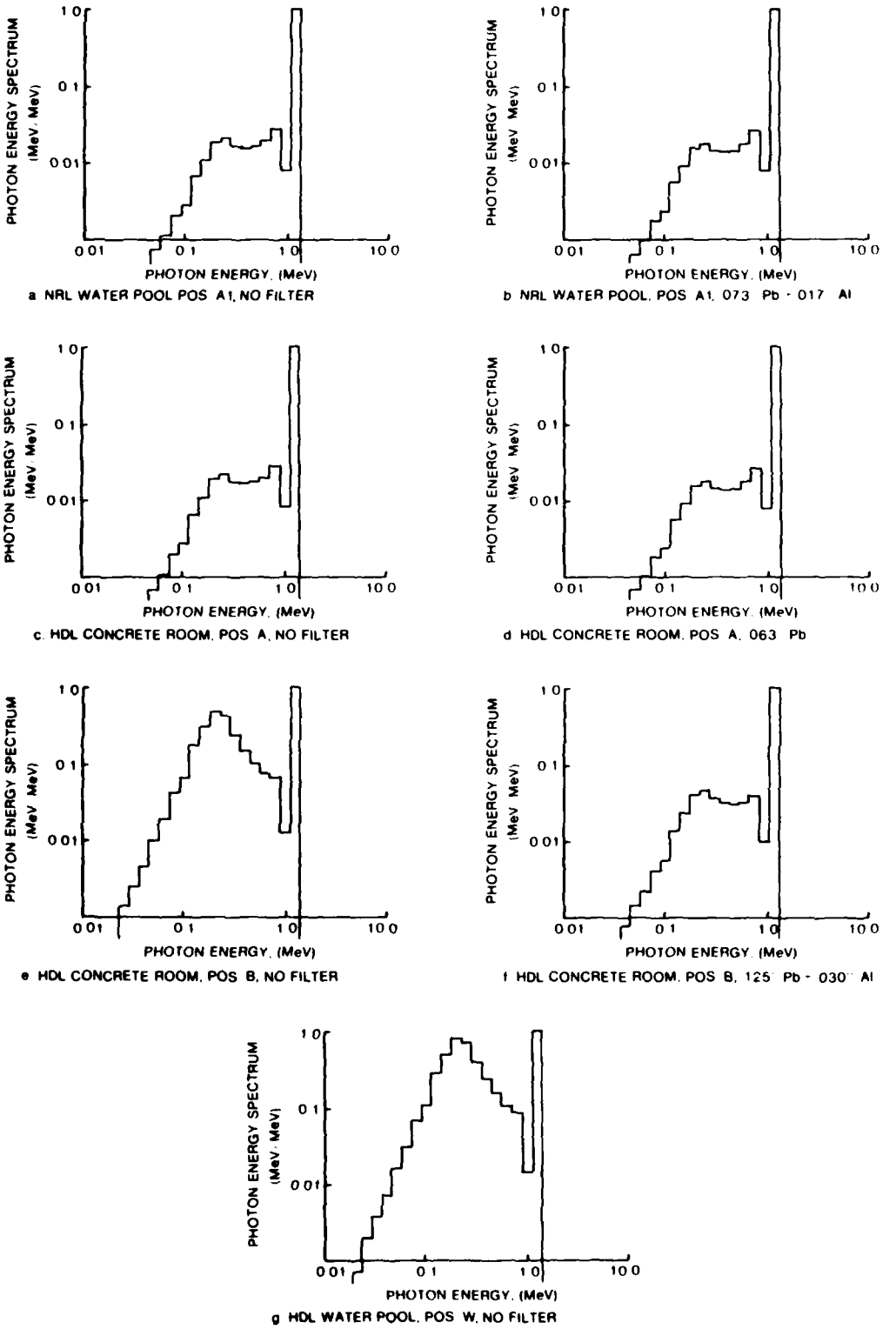

Figure 8. Measured cobalt-60 source spectra: differential absorption TLD measurements.

last place into group II because of much heavier filtering (0.125-in. Pb versus 0.063-in. Pb), while line 5 probably moved into last place because of the very thick aluminum layer in the filter which contributes a lot of scatter of its own. However, all three of these high-scatter geometries moved from group IV into, at worst, group III.

TABLE 4. RELATIVE RANKING OF UNFILTERED COBALT-60 SOURCES IN ORDER OF DECREASING SPECTRAL HARDNESS

Line No.	Cobalt-60 source configuration				Unfiltered I_{Au}/I_{Al}	Quality factor
	Place	Type	Position	Figure		
10	NBS	Teletherapy source	--	5a	2.18	I
6	HDL	Concrete room	A	4a	2.70	
1	NRL	Water well	A1	3a	2.71	II
8	NASA	Concrete room	A	4b	2.93	
2	NBS	Water well	--	3a	2.98	
3	HDL	Water well	B	3a	3.23	
11	NASA	Gammacell™-220	--	5b	3.53	III
4	NRL	Water well	A5	3b	3.86	
9	NASA	Concrete room	B	4b	6.17	
5	HDL	Water well	W	3b	7.40	IV
7	HDL	Concrete room	B	4a	7.56	

TABLE 5. RELATIVE RANKING OF FILTERED COBALT-60 SOURCES IN ORDER OF DECREASING SPECTRAL HARDNESS

Line No.	Cobalt-60 source configuration				Filter		Filtered I_{Au}/I_{Al}	Quality factor
	Place	Type	Position	Figure	Pb (in.) + Al (in.)			
1	NRL	Water well	A1	3a	0.073	0.017	2.02	
2	NBS	Water well	--	3a	0.063	0.030	2.04	
10	NBS	Teletherapy source	--	5a	0.063	0.030	2.07	
3	HDL	Water well	B	3a	0.063	0.030	2.11	I
6	HDL	Concrete room	A	4a	0.063	0.000	2.12	
11	NASA	Gammacell™-220	--	5b	0.063	0.030	2.17	
8	NASA	Concrete room	A	4b	0.063	0.030	2.21	
4	NRL	Water well	A5	3b	0.073	0.017	2.28	
7	HDL	Concrete room	B	4a	0.125	0.030	2.52	II
9	NASA	Concrete room	B	4b	0.063	0.030	3.27	III
5	HDL	Water well	W	3b	0.063	0.125	3.53	

7. INTERFACE DOSE ENHANCEMENT

Since the actual phenomenon of interest is the degree of interface dose enhancement which might be expected for a given cobalt-60 source spectrum, it is important to know whether the ionization chamber measurement can be related to a dose-enhancement factor. In the following discussion, dose-enhancement factor, F_{DE}, is taken to mean the dose in a low-Z material at the interface with a high-Z material divided by the equilibrium dose in the low-Z material. Specifically, we propose the following procedure:

(a) Determine the ionization chamber response ratio, I_{Au}/I_{Al}, for a cobalt-60 source configuration of interest.

(b) Find an "effective" monoenergetic photon energy, E_{eff}, corresponding to this ionization chamber response ratio from figure 2.

(c) Using published values of F_{DE} versus E_γ,[6] or calculating F_{DE} using the simplified model of Chadsey,[7] find the dose-enhancement factor at the effective energy E_{eff} for the material combination of interest (an abbreviated version of Chadsey's simplifed dose-enhancement model is given in app B).

In order to test the validity of this procedure, we calculated an estimated dose enhancement factor, F_{DE}, in Si at an Si/Au interface using steps (a) to (c) above. For the monoenergetic dose-enhancement factor, F_{DE} versus E_γ, we used Garth and Chadsey's POEM calculation for Si/Au (figure 1 of Garth et al[6]). The results of this procedure are given in table 6 for all the ionization chamber measurements given in table 1. Note that the dose enhancement factor for a pure monoenergetic 1.25-MeV cobalt-60 gamma would be 1.68.

TABLE 6. ESTIMATED DOSE ENHANCEMENT FACTORS, F_{DE}(Si/Au)

Line No.	Cobalt-60 source configuration				Unfiltered F_{DE}	Filter		Filtered F_{DE}
	Place	Type	Position	Figure		Pb (in.)	+ Al (in.)	
1	NRL	Water well	A1	3a	1.86	0.073	0.017	1.73
2	NBS	Water well	--	3a	1.91	0.063	0.030	1.76
3	HDL	Water well	B	3a	1.96	0.063	0.030	1.74
4	NRL	Water well	A5	3b	2.09	0.073	0.017	1.77
5	HDL	Water well	W	3b	2.97	0.063	0.125	2.02
6	HDL	Concrete room	A	4a	1.86	0.063	0.000	1.74
7	HDL	Concrete room	B	4a	3.02	0.125	0.030	1.83
8	NASA	Concrete room	A	4b	1.91	0.063	0.000	1.87
9	NASA	Concrete room	B	4b	2.62	0.063	0.030	1.97
10	NBS	Teletherapy source	--	5a	1.76	0.063	0.030	1.73
11	NASA	Gammacell™-220	--	5b	2.02	0.063	0.030	1.75

[6] J. C. Garth, W. L. Chadsey, and R. L. Sheppard, Jr., IEEE Trans. Nucl. Sci., NS-22 (1975), 2562.

[7] W. L. Chadsey, IEEE Trans. Nucl. Sci., NS-25 (1978), 1591.

For cobalt-60 source configurations for which the spectrum is known (or thought to be known) we can calculate the dose-enhancement factor by integrating F_{DE} versus E_γ over the photon spectrum in a manner similar to the integration given in equation (14). Calculated dose-enhancement factors for the spectra calculated by Woolf are given in table 7. Similarly calculated dose-enhancement factors for the spectra determined by TLD differential absorption measurements are given in table 8. The agreement between the dose-enhancement factors estimated from ionization chamber measurements and the "true" calculated dose-enhancement factors is very good. The ionization chamber technique underestimates the true dose-enhancement factor by 9 percent.

TABLE 7. COMPARISON OF F_{DE} VALUES ESTIMATED FROM IONIZATION CHAMBER MEASUREMENTS WITH THOSE CALCULATED FROM MONTE-CARLO SPECTRA (ref 3,4)

Line No.	Cobalt-60 source configuration				Filter			Figure[b]
	Place	Type	Position	Figure[a]	Pb + Al (in.) (in.)	Estimated F_{DE}	Calculated F_{DE}	
2	NBS	Water well	--	3a	(Unfiltered)	1.91	2.16	7g
5	HDL	Water well	W	3b	(Unfiltered)	2.97	3.08	7a
					0.063 0.125	2.02	2.09	7b
6	HDL	Concrete room	A	4a	(Unfiltered)	1.86	1.98	7c
					0.063 0.000	1.74	1.76	7d
7	HDL	Concrete room	B	4a	(Unfiltered)	3.02	3.51	7e
					0.125 0.030	1.83	1.78	7f
11	NASA	Gammacell™-220	--	5b	(Unfiltered)	2.02	2.57	7h

[a]Figure showing source configuration.
[b]Figure showing calculated spectrum.

TABLE 8. COMPARISON OF F_{DE} VALUES ESTIMATED FROM IONIZATION CHAMBER MEASUREMENTS WITH THOSE CALCULATED FROM MEASURED COBALT-60 SPECTRA

Line No.	Cobalt-60 source configuration				Filter			Figure[b]
	Place	Type	Position	Figure[a]	Pb + Al (in.) (in.)	Estimated F_{DE}	Calculated F_{DE}	
1	NRL	Water well	A1	3a	(Unfiltered)	1.86	1.88	8a
					0.073 0.017	1.73	1.86	8b
5	HDL	Water well	W	3b	(Unfiltered)	2.97	4.54	8g
6	HDL	Concrete room	A	4a	(Unfiltered)	1.86	1.88	8c
					0.063 0.000	1.74	1.86	8d
7	HDL	Concrete room	B	4a	(Unfiltered)	3.02	3.76	8e
					0.125 0.030	1.83	2.00	8f

[a]Figure showing source configuration.
[b]Figure showing measured spectrum.

8. CONCLUSIONS

The gold- and aluminum-walled ionization chamber measurement yields a simple and easy assessment of the magnitude of the low-energy scattered component of a given cobalt-60 irradiator spectrum. While a complete gamma spectrum cannot be determined using this method, it does yield a measure of the gold and aluminum equilibrium dose rates. These are directly related to the relative magnitude of the interface dose-enhancement effect to be expected in a microelectronic device irradiation.

The gold/aluminum ionization chamber technique yields an immediate quantitative indication of the degree of dose enhancement which can be achieved by any given filter combination for a particular source configuration.

The results clearly identify the types of source configurations which have inherently high scatter. The results also provide empirical evidence that the spectra of most practical cobalt-60 irradiators can be hardened to equal or better that of the best available unscattered spectrum, if the test object is enclosed in a filter box consisting of 0.063 in. of lead on the source side, followed by no more than 0.030 in. of aluminum. The experimental data seem to indicate that smaller thicknesses of aluminum are better, and that no aluminum may be best.

ACKNOWLEDGEMENTS

It is a pleasure to thank James Humphreys of the National Bureau of Standards for making his water well and teletherapy sources available for these experiments, and Vitaly Danchenko and Sidney Brashears for likewise allowing me to use their concrete room source and their Gammacell™-220. Finally I would like to thank Edward A. Burke of Mission Research Corporation for the initial idea, and for helpful suggestions during the course of this research.

LITERATURE CITED

(1) L. F. Lowe, J. R. Capelli, and E. A. Burke, IEEE Trans. Nucl. Sci., NS-29 (1982), 1992.

(2) J. C. Garth, E. A. Burke, and S. Woolf, IEEE Trans. Nucl. Sci., NS-27 (1980), 1459.

(3) S. Woolf and A. R. Frederickson, IEEE Trans. Nucl. Sci., NS-30 (1983), 4371.

(4) S. Woolf and E. A. Burke, IEEE Trans. Nucl. Sci., NS-31 (1984), 1089.

(5) J. A. Wall and E. A. Burke, IEEE Trans. Nucl. Sci., NS-17, No. 6 (December 1970), 305.

(6) J. C. Garth, W. L. Chadsey, and R. L. Sheppard, Jr., IEEE Trans. Nucl. Sci., NS-22 (1975), 2562.

(7) W. L. Chadsey, IEEE Trans. Nucl. Sci., NS-25 (1978), 1591.

(8) D. B. Brown and C. M. Dozier, IEEE Trans. Nucl. Sci., NS-29 (1982), 1996.

(9) D. M. Long, D. G. Millward, and J. Wallace, IEEE Trans. Nucl. Sci., NS-29 (1982), 1980.

(10) T. E. Burlin, The Theory of Dosimeter Response with Particular Reference to Ionization Chambers, chapter II in Manual on Radiation Dosimetry, ed. by N. W. Holm and R. J. Berry, Marcel Dekker Inc., New York (1970), p 27.

(11) J. W. Boag, Ionization Chambers, chapter 9 in Radiation Dosimetry, ed. by F. H. Attix and W. C. Roesch, 2nd edition, vol. II, Academic Press, New York (1966), p 16.

(12) R. D. Evans, The Atomic Nucleus, McGraw-Hill, New York (1955), p 725.

(13) Radiation Dosimetry: X-Rays and Gamma Rays with Maximum Photon Energies Between 0.6 and 50 MeV, International Commission on Radiation Units and Measurements, ICRU Report 14, Washington (1969), p 4.

(14) R. D. Evans, X-Ray and γ-Ray Interactions, chapter 3 in Radiation Dosimetry, ed. by F. H. Attix and W. C. Roesch, 2nd edition, vol I, Academic Press, New York (1968), p 125 ff.

(15) J. H. Hubbell, Trends in Radiation Dosimetry, 33, No. 11 (November 1982).

(16) M. J. Berger and S. M. Seltzer, Tables of Energy Losses and Ranges of Electrons and Positrons, National Aeronautics and Space Administration, NASA SP-3012, Washington (1964).

APPENDIX A.--DRAWINGS OF IONIZATION CHAMBER

Complete production drawings for the ionization chamber are given in this appendix.

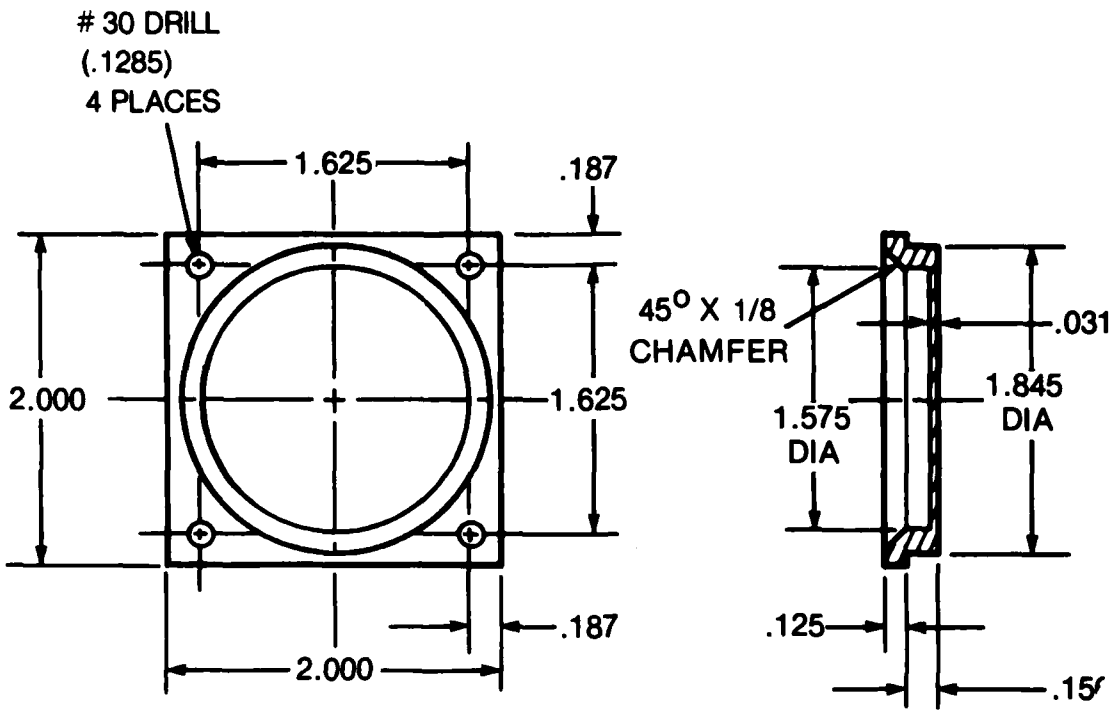

MATERIAL: LEXAN
QUANTITY REQUIRED: 2

COVER

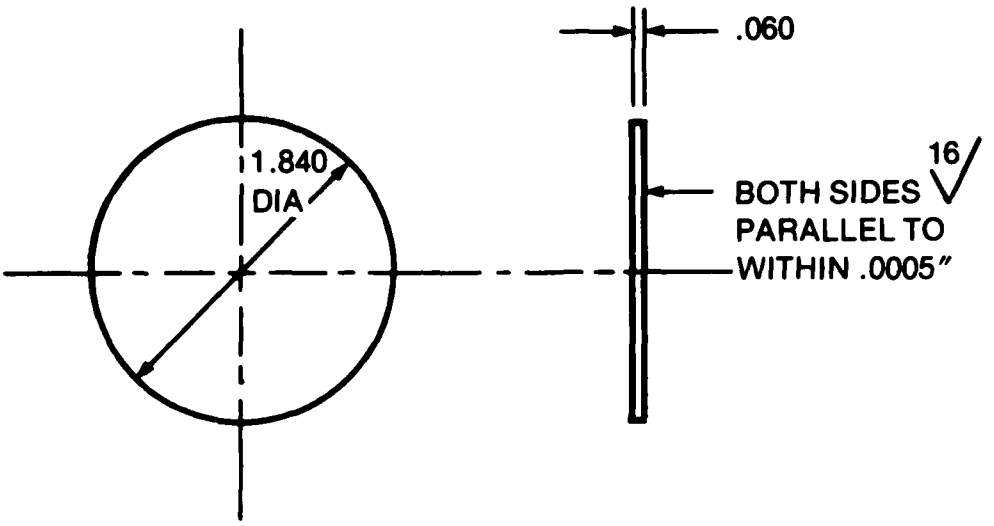

MATERIAL: ALUMINUM ALLOY 7075

QUANTITY REQUIRED: 4

NOTE:

2 PIECES PLAIN
2 PIECES WITH .002" GOLD FOIL BONDED TO ONE SIDE
USE EASTMAN 910 OR LOCTITE 496 CYANOACRYLATE ESTER ADHESIVE.

ELECTRODE

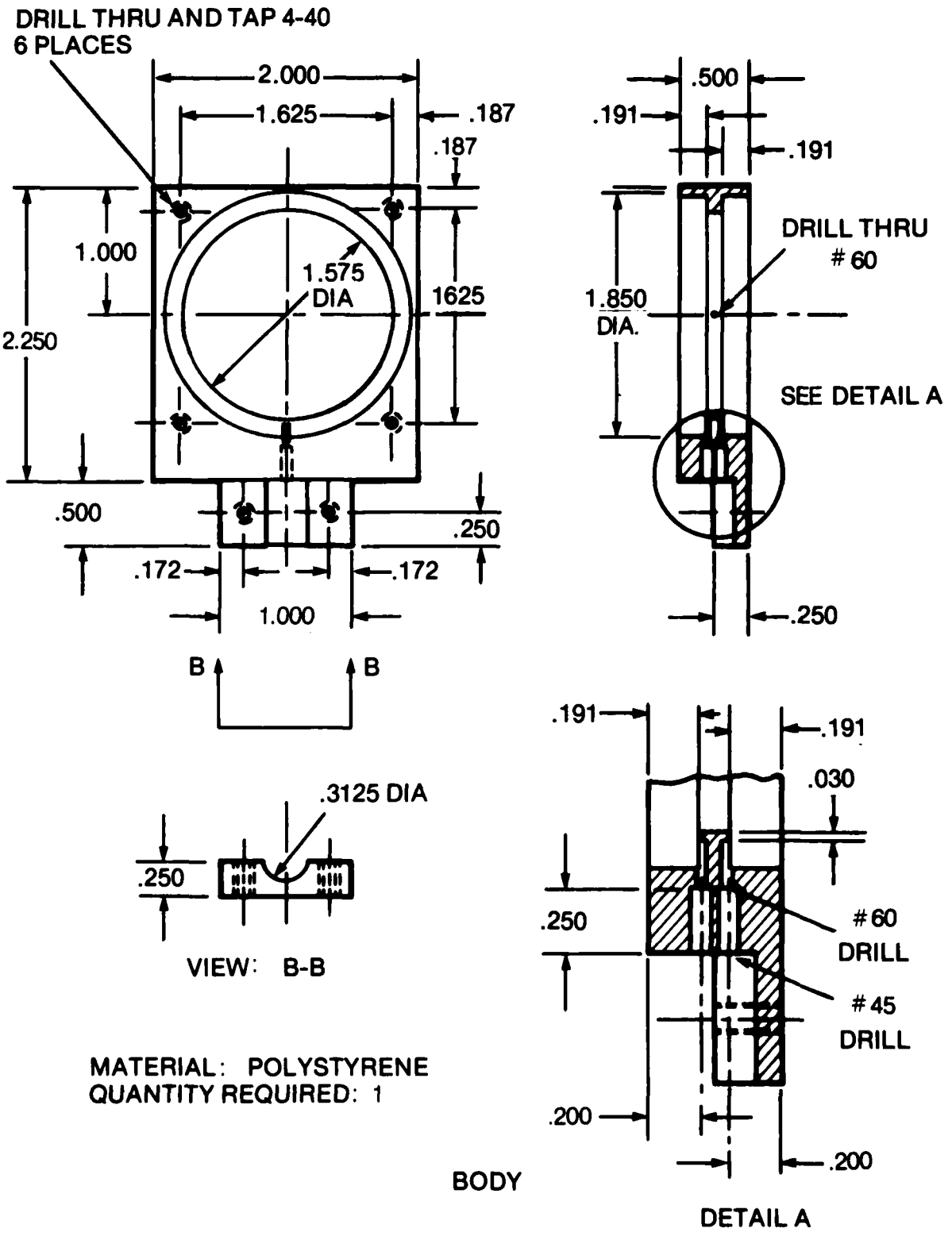

MATERIAL: POLYSTYRENE
QUANTITY REQUIRED: 1

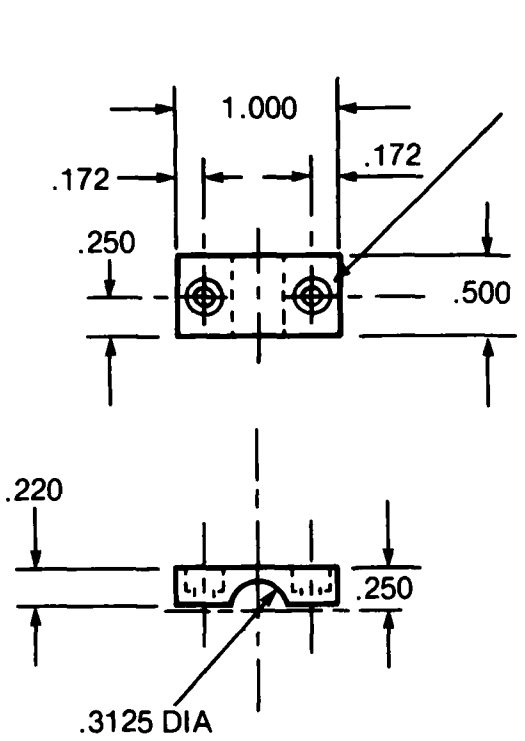

MATERIAL: ALUMINUM
QUANTITY REQUIRED: 1

CLAMP

APPENDIX A

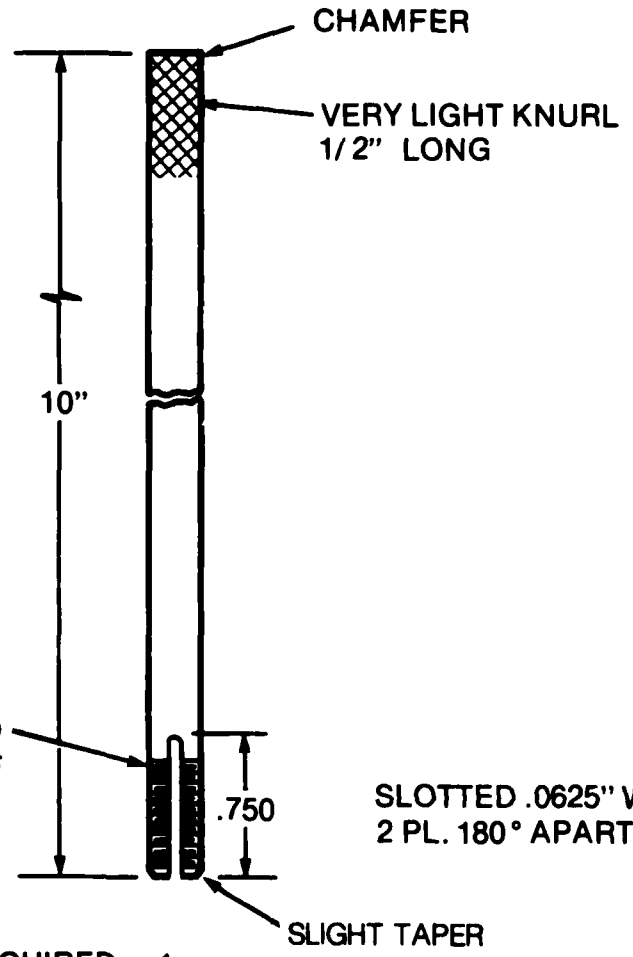

QUANTITY REQUIRED: 1

MAKE FROM: 5/16 O.D. x 1/4 I.D.
ALUMINUM TUBING

STEM

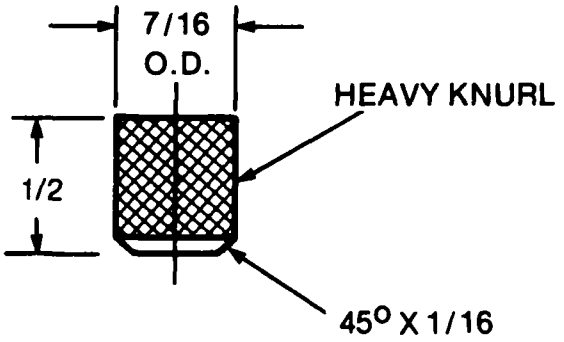

NOTE:
5/16-24 UNF INTERNAL THREAD
AND TAPER TO MATCH STEM

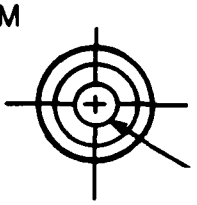

MATERIAL: NICKEL PLATED BRASS

CABLE CLAMPING NUT

APPENDIX B.--SIMPLE DOSE-ENHANCEMENT MODEL

Abstracted from W. Chadsey, IEEE Trans. Nucl. Sci. NS-25 (1978), 1591

This simplified dose-enhancement model can be used in combination with ionization chamber measurements to estimate an upper limit for the dose-enhancement factor for a specific combination of material layers and cobalt-60 source configuration (see sect. 7 in the body of the report).

Let 1 refer to a high-Z material (e.g., Au).

Let 2 refer to a low-Z material (e.g., Si).

Let F_{DE}, the dose-enhancement factor, be the dose in material 2 at the interface with material 1 divided by the equilibrium dose in material 2.

Then

$$F_{DE} = f_1 + f_2 \frac{R_1}{R_2} \frac{(\mu_{en}/\rho)_1}{(\mu_{en}/\rho)_2} ,$$

where

$$f_1 = (1 - \beta_1)(1 + \beta_2)/2(1 - \beta_1\beta_2),$$

$$f_2 = (1 - \beta_2)(1 + \beta_1)/2(1 - \beta_1\beta_2),$$

$$\beta_Z = 90.475Z^{0.177} - 0.40,$$

R_Z = electron range in material Z (g/cm^2), and

$(\mu_{en}/\rho)_Z$ = mass energy absorption coefficient in material Z (cm^2/g).

Using this simple model, the dose enhancement as a function of photon energy, E_γ, can be calculated for any combination of materials, $4 \leq Z \leq 82$, from readily available tabulated range and mass energy absorption coefficient data.

DISTRIBUTION

ADMINISTRATOR
DEFENSE TECHNICAL INFORMATION CENTER
ATTN DTIC-DDA (12 COPIES)
CAMERON STATION, BUILDING 5
ALEXANDRIA, VA 22304-6145

COMMANDER
US ARMY COMBAT SYSTEMS
TEST ACTIVITY
ATTN C. HEIMBACH
BLDG 860 STECS-NE
ABERDEEN PROVING GROUND, MD 21005-5059

NVEOL
ATTN DELNV-IRT, A. J. KENNEDY
FT BELVOIR, VA 22060

WSMR
PO BOX 234
ATTN T. M. FLANDERS
WHITE SANDS, NM 88002

WHITE SANDS MISSILE RANGE
PO BOX 215
ATTN DR. J. MEASON
WHITE SANDS MISSILE RANGE, NM 88002

WHITE SANDS MISSILE RANGE
PO BOX 333
ATTN DR. W. W. SALLEE
WHITE SANDS, NM 88002

NAVAL RESEARCH LABORATORY
REACTOR MATERIALS BRANCH
ATTN CODE 6290, L. E. STEELE, HEAD
WASHINGTON, DC 20375

NAVAL RESEARCH LABORATORY
ATTN CODE 6680, DR. DENNIS BROWN
ATTN CODE 6464, F. J. CAMPBELL
ATTN CODE 6682, DR. C. M. DOZIER
ATTN CODE 6070, S. G. GORBICS, (20 COPIES)
WASHINGTON, DC 20375

RADC/ESR
ATTN J. C. GARTH
HANSCOM AFB, MA 01731

NASA GODDARD SPACE FLIGHT CENTER
ATTN CODE 754, V. DANCHENKO
ATTN CODE 754, S. BRASHEARS
GREENBELT, MD 20771

NASA LANGLEY RESEARCH CENTER
ATTN SHIELA ANN L. LONG
MS 399
HAMPTON, VA 23665

BATTELLE PACIFIC NORTHWEST LABORATORY
PO BOX 999
ATTN DR. P. L. ROBERSON
SENIOR RESEARCH SCIENTIST
RADIOLOGICAL SCIENCE DEPARTMENT
318 BUILDING, 300 AREA
RICHLAND, WA 99352

BALLISTIC RESEARCH LABS
ATTN A. H. KAZI
ABERDEEN, MD 21001

HANFORD ENGINEERING DEVELOPMENT LAB
PO BOX 1970
ATTN DR. W. N. McELROY
CHAIRMAN, ASTM E10.05
300 AREA
RICHLAND, WA 99352

JPL
M/S T-1180
ATTN M. GAUTHIER
4800 OAK GROVE DRIVE
PASADENA, CA 91109

JET PROPULSION LABORATORY
ATTN J. W. WINSLOW
MS 144-218
4800 OAK GROVE DRIVE
PASADENA, CA 91103

JET PROPULSION LABORATORY
CALIFORNIA INSTITUTE OF TECHNOLOGY
ATTN W. E. PRICE
ATTN S. SOLI
4800 OAK GROVE DRIVE
PASADENA, CA 91109

MAXWELL LABS, INC
ATTN J. E. RAUCH
9244 BALBOA AVE
SAN DIEGO, CA 92123

PACIFIC NORTHWEST LAB
PO BOX 999
ATTN W. C. MORGAN
RICHLAND, WA 99352

PNL
PO BOX 999
ATTN DR. J. L. BRIMHALL
RICHLAND, WA 99352

RISO NATIONAL LABORATORY
ACCELERATOR DEPARTMENT
PO BOX 49
ATTN DR. A. MILLER
DK-4000 ROSKILDE, DENMARK

SANDIA LABS.
PO BOX 5800
ATTN W. H. BUCKELEW, ORG. 6446
ATTN DR. J. A. HALBLEIB, SR, DIV 4231
ATTN J. G. KELLY, DIV. 1232
ATTN DR. T. F. LUERA, DIV 6451
ATTN L. D. POSEY, DIV 1232
ALBUQUERQUE, NM 87185

SANDIA NATIONAL LABORATORIES
RADIATION DOSIMETRY LABORATORY
EXPERIMENTAL SYSTEMS DESIGN
DIVISION 6452
ATTN DR. D. W. VEHAR
ALBUQUERQUE, NM 87185

AECL RADIOCHEMICAL COMPANY
SENIOR RADIATION PHYSICIST
PO BOX 13500
ATTN R. CHU
KANATA, ONT, CANADA K2K 1X8

AEROJET NUCLEAR CE
ATTN J. M. BEESTON
1604 CHARLENE STREET
IDAHO FALLS, ID 83401

ARACOR
ATTN L. J. PALKUTI
1223 E. ARQUES AVE
SUNNYVALE, CA 94086

ARCON CORPORATION
ATTN S. WOOLF
260 BEAR HILL ROAD
WALTHAM, MA 02154

ATOMIC ENERGY OF CANADA, LTD.
PO BOX 6300, STATION J
ATTN B. J. JACKSON
OTTAWA, CANADA K2A 3W3

ATOMIC ENERGY OF CANADA, LTD.
ATTN DR. K. MEHTA
PINAWA, MANITOBA
CANADA ROE 1LO

BABCOCK & WILCOX CO
PO BOX 1260
ATTN R. H. LEWIS
LYNCHBURG, VA 24505

BATTELLE PROJECT MANAGEMENT DIV
ATTN DR. J. PERRIN
505 KING AVENUE
COLUMBUS, OH 43201

BOEING COMPANY
ATTN ROGER C. KENNEDY
MS 2R-GV, PO BOX 3999
SEATTLE, WA 98124

BOEING AEROSPACE CO
ORGN 2-5310, MS 2R-00
ATTN R. GUAY
SEATTLE, WA 98124

BOEING CO
ATTN RONALD FUSCH
MS 2R-GV, PO BOX 3999
SEATTLE, WA 98124

BOEING AEROSPACE CO
PO BOX 3999
ATTN ITSU ARIMURA
SEATTLE, WA 98124

GENERAL MANAGER
RADIATION-STERILIZERS, INC
ATTN DR. B. P. FAIRAND
305 ENTERPRISE DRIVE
WESTERVILLE, OH 43081

HUGHES AIRCRAFT
ATTN K. R. WALKER
BLDG. 700, MS A2408
NEWPORT BEACH, CA 92663

IRT CORPORATION
LINAC FACILITY
ATTN D. E. WILLIS, MANAGER
7695 FORMULA PLACE
SAN DIEGO, CA 92121

IRT CORP
PO BOX 80817
ATTN J. HARRITY
SAN DIEGO, CA 92138

JAYCOR
PO BOX 85154
ATTN DR. B. C. PASSENHEIM
11011 TORREYANA ROAD
SAN DIEGO, CA 92138

JOHNSON & JOHNSON RESEARCH
ATTN T. A. OLEJNIK
21 LAKE DRIVEE. WINDSOR, NJ 08520

KAMAN-TEMPO
ATTN DR. E. WOLICKI
2560 HUNTINGTON AVENUE
SUITE 500
ALEXANDRIA, VA 22303

KAMAN TEMPO
ATTN W. A. ALFONTE
2560 HUNTINGTON AVE
SUITE 506
ALEXANDRIA, VA 22303

G. MESSENGER
3111 BEL AIR DRIVE
LAS VEGAS, NV 89109

MISSION RESEARCH CORP
ATTN E. A. BURKE
74 NORTHEASTERN BLVD
NASHUA, NH 03062

MISSION RESEARCH CORPORATION
ATTN DR. E. A. BURKE
11 INDIAN HILL ROAD
WOBURN, MA 01801

NORTHROP CORPORATION
ONE RESEARCH PARK
ATTN DR. J. R. SROUR
PALOS VERDES PENINSULA, CA 90274

NORTHROP CORPORATION
ELECTRONICS DIVISION
ATTN B. T. AHLPORT
2301 W. 120TH STREET
HAWTHORNE, CA 90250

RADIATION DYNAMICS INC.
ENGINEERING DEPARTMENT
ATTN M. STRELCZYK
EXPERIMENTAL APPLICATIONS PHYSICIST
316 SOUTH SERVICE RD
MELVILLE, NY 11747

RAYTHEON CO
EQUIPMENT DEVELOPMENT LABORATORIES
ATTN R. N. DIETTE
ATTN B. W. SCHUPP
528 BOSTON POST ROAD
SUDBURY, MA 01776

ROCKWELL
PO BOX 1449
ATTN P. S. OLSON
CANOGA PARK, CA 91304

ROCKWELL INTERNATIONAL
MANAGER, APPLIED NUCLEAR RESEARCH
ROCKETDYNE DIVISION, NA02
ATTN DR. H. FARRAR IV
6633 CANOGA AVENUE
CANOGA PARK, CA 91304

SCIENCE APPLICATIONS, INC
ATTN DR. V. V. VERBINSKI
1200 PROSPECT STREET
LA JOLLA, CA 93027

TRW DEFENSE SYSTEMS GROUP
ONE SPACE PARK
ATTN R. D. LOVELAND
REDONDO BEACH, CA 90278

UNION CARBIDE COMPANY
NUCLEAR DIVISION
PO BOX X
ATTN F. B. K. KAM
OAK RIDGE, TN 37830

WESTINGHOUSE HANFORD CO
ATTN H. R. BRAGER
326 BLD. W/A-57, BOX 1970
RICHLAND, WA 99352

WESTINGHOUSE HANFORD CO
ATTN DR. F. A. GARNER
326 BLDG 300, AREA W/a-57
RICHLAND, WA 99352

WESTINGHOUSE HANFORD CO
BOX 1970
ATTN F. R. SHOBER
RICHLAND, WA 99352

UNIVERSITY OF ARKANSAS
MECHANICAL ENGINEERING DEPARTMENT
ATTN DR. J. G. WILLIAMS
FAYETTEVILLE, AR 72701

UNIVERSITY OF MARYLAND
INSTITUTE FOR PHYSICAL SCIENCE
TECHNOLOGY
ATTN DR. W. J. CHAPPAS
COLLEGE PARK, MD 20742

NATIONAL BUREAU OF STANDARDS
ATTN DR. R. S. CASWELL, 245/B109
ATTN DR. S. E. CHAPPELL, ADMIN/A625
ATTN W. L. McLAUGHLIN, 245/C216
ATTN DR. J. W. MOTZ, 245/C216
ATTN J. C. HUMPHREYS, 245/C216
GAITHERSBURG, MD 20899

US ARMY LABORATORY COMMAND
ATTN COMMANDER, AMSLC-CG
ATTN TECHNICAL DIRECTOR, AMSLC-TD

INSTALLATION SUPPORT ACTIVITY
ATTN DIRECTOR, SLCIS-D
ATTN RECORD COPY, SLCIS-IM-TS
ATTN LIBRARY, SLCIS-IM-TL (3 COPIES)
ATTN LIBRARY, SLCIS-IM-TL (WOODBRIDGE)
ATTN TECHNICAL REPORTS BRANCH, SLCIS-IM-TR
ATTN LEGAL OFFICE, SLCIS-CC

DISTRIBUTION (Cont'd)

HARRY DIAMOND LABORATORIES
ATTN D/DIVISION DIRECTORS
ATTN DIVISION DIRECTOR, SLCHD-RT
ATTN CHIEF, SLCHD-NW-P
ATTN J. R. ROSADO, SLCHD-NW
ATTN S. SHARE, SLCHD-NW-RA
ATTN W. VAULT, SLCHD-NW-RA
ATTN J. BENEDETTO, SLCHD-NW-RC
ATTN H. BOESCH, SLCHD-NW-RC
ATTN J. McGARRITY, SLCHD-NW-RC
ATTN F. McLEAN, SLCHD-NW-RC
ATTN T. OLDHAM, SLCHD-NW-RC
ATTN M. BUMBAUGH, SLCHD-NW-RH
ATTN H. EISEN, SLCHD-NW-RH
ATTN J. HALPIN, SLCHD-NW-RH
ATTN R. GILBERT, SLCHD-NW-RH
ATTN J. BLACKBURN, SLCHD-NW-RH
ATTN G. MERKEL, SLCHD-NW-RH
ATTN S. RATTNER, SLCHD-NW-RH
ATTN C. SELF, SLCHD-NW-RH
ATTN F. J. AGEE, SLCHD-NW-RI
ATTN C. CASAER, SLCHD-NW-RI
ATTN D. DAVIS, SLCHD-NW-RI
ATTN S. GRAYBILL, SLCHD-NW-RI
ATTN G. HUTTLIN, SLCHD-NW-RI
ATTN P. SARIGIANIS, SLCHD-NW-RI
ATTN D. WHITTAKER, SLCHD-NW-RI
ATTN K. KERRIS, SLCHD-NW-RI (100 COPIES)

SUPPLEMENTARY

INFORMATION

DEPARTMENT OF THE ARMY
HEADQUARTERS, U.S. ARMY LABORATORY COMMAND
2800 POWDER MILL RD., ADELPHI, MD 20783-1145

REPLY TO
ATTENTION OF

SLCHD-NW-RI

TO: Recipients of HDL-TR-2082
FROM: Klaus G. Kerris, SLCHD-NW-RI
SUBJECT: HDL-TR-2082, Experimental Determination of the Low-Energy Spectral Component of Cobalt-60 Sources, by Kerris and Gorbics, dated April 1986.

This copy should replace page 37 of the above-described HDL report.

APPENDIX B.--SIMPLE DOSE-ENHANCEMENT MODEL

Abstracted from W. Chadsey, IEEE Trans. Nucl. Sci. NS-25 (1978), 1591

This simplified dose-enhancement model can be used in combination with ionization chamber measurements to estimate an upper limit for the dose-enhancement factor for a specific combination of material layers and cobalt-60 source configuration (see sect. 7 in the body of the report).

Let 1 refer to a high-Z material (e.g., Au).

Let 2 refer to a low-Z material (e.g., Si).

Let F_{DE}, the dose-enhancement factor, be the dose in material 2 at the interface with material 1 divided by the equilibrium dose in material 2.

Then

$$F_{DE} = f_2 + f_1 \frac{R_1}{R_2} \frac{(\mu_{en}/\rho)_1}{(\mu_{en}/\rho)_2} ,$$

where

$$f_1 = (1 - \beta_1)(1 + \beta_2)/2(1 - \beta_1\beta_2),$$

$$f_2 = (1 - \beta_2)(1 + \beta_1)/2(1 - \beta_1\beta_2),$$

$$\beta_Z = 0.475Z^{0.177} - 0.40,$$

R_Z = electron range in material Z (g/cm^2), and

$(\mu_{en}/\rho)_Z$ = mass energy absorption coefficient in material Z (cm^2/g).

Using this simple model, the dose enhancement as a function of photon energy, E_γ, can be calculated for any combination of materials, $4 \leq Z \leq 82$, from readily available tabulated range and mass energy absorption coefficient data.